Aerosol Science and Technology

ISSN: 0278-6826 (Print) 1521-7388 (Online) Journal homepage: https://www.tandfonline.com/loi/uast20

Investigation of the absorption Ångström exponent and its relation to physicochemical properties for mini-CAST soot

Sandra Török, Vilhelm B. Malmborg, Johan Simonsson, Axel Eriksson, Johan Martinsson, Manu Mannazhi, Joakim Pagels & Per-Erik Bengtsson

To cite this article: Sandra Török, Vilhelm B. Malmborg, Johan Simonsson, Axel Eriksson, Johan Martinsson, Manu Mannazhi, Joakim Pagels & Per-Erik Bengtsson (2018) Investigation of the absorption Ångström exponent and its relation to physicochemical properties for mini-CAST soot, Aerosol Science and Technology, 52:7, 757-767, DOI: 10.1080/02786826.2018.1457767

To link to this article: https://doi.org/10.1080/02786826.2018.1457767

AEROSOL SCIENCE AND TECHNOLOGY
2018, VOL. 52, NO. 7, 757–767
https://doi.org/10.1080/02786826.2018.1457767

Investigation of the absorption Ångström exponent and its relation to physicochemical properties for mini-CAST soot

Sandra Török[a], Vilhelm B. Malmborg[b], Johan Simonsson[a], Axel Eriksson[b], Johan Martinsson[c], Manu Mannazhi[a], Joakim Pagels[b], and Per-Erik Bengtsson[a]

[a]Division of Combustion Physics, Lund University, Lund, Sweden; [b]Division of Ergonomics and Aerosol Technology, Lund University, Lund, Sweden; [c]Division of Nuclear Physics, Lund University, Lund, Sweden

ABSTRACT

In this work, a mini-CAST soot generator was used to produce soot with different optical and physicochemical characteristics. Absorption Ångström exponents (*AAE*) expressing the absorption wavelength dependence were assessed by multiwavelength *in-situ* and filter-based (aethalometer) laser extinction. The two optical techniques showed good agreement. For the chosen mini-CAST operating conditions, *AAE*s between 1 and 3.5 were found. Soot with high mass-fractions of organic carbon (OC) and pyrolytic carbon (PC) determined with thermal optical analysis were associated with *AAE*s significantly higher than 1. Heating to 250 and 500°C removed the majority of polycyclic aromatic hydrocarbons. However, the thermal-optical analysis revealed that OC and PC were abundant in the soot with $AAE > 2$ also after heating the aerosol. Analysis of mass absorption cross section ratios for elemental carbon and OC indicated that elevated *AAE*s also after heating to 500°C could be related to persistent OC and PC components and/or the refractory soot. By comparing the mini-CAST soot optical properties with soot properties derived from *in-situ* extinction measurements in a premixed flame, mini-CAST soot with a higher *AAE* could be identified as less mature soot.

ARTICLE HISTORY
Received 31 August 2017
Accepted 2 March 2018

EDITOR
Matti Maricq

1. Introduction

Soot particles are formed as a result of incomplete combustion, for example in forest fires, internal combustion engines, power plants, and indoor open fire cooking. Their physicochemical and optical properties depend on, and can vary significantly, with the combustion process from which they originate (Wang 2011; Bockhorn 2013). A rapid cooling to ambient temperatures occurs after soot is emitted to the atmosphere from a combustion process at high temperature. During this cooling process, semivolatile and low-volatile substances in the exhaust condense on soot surfaces. Soot is, therefore, often described as consisting of a carbonaceous core (which formed inside the flame) and an organic part (which condenses on particles outside the flame) consisting of semivolatile organic compounds, including polycyclic aromatic hydrocarbons (PAHs) (Canagaratna et al. 2015) which to various degrees are mutagenic and carcinogenic (Boström et al. 2002; Janssen et al. 2012; Kennedy 2007).

As soot particles are very efficient absorbers of solar radiation (Bond and Bergstrom 2006), soot contributes directly to the radiative forcing of the earth. Soot, or black carbon (BC) as it is most often termed in climate-related discussions, is one of the main contributors to radiative forcing after carbon dioxide (Bond et al. 2013; IPCC 2013). Recently, attention has also been directed to the importance of absorption by light-absorbing organic aerosols, brown carbon (BrC), in the atmosphere (Saleh et al. 2014; Liu et al. 2015; Cappa et al. 2012; Liu et al. 2017). This class of organic carbon (OC), mainly associated with biomass burning, absorbs strongly in the ultraviolet spectral region. The great uncertainty concerning the importance of brown carbon in atmospheric radiative forcing motivates extensive research on the matter.

Soot formation processes are intrinsically complex, and occur in fuel-rich regions of flames at elevated temperatures (see Wang 2011 and references therein). Here fuel fragments build larger hydrocarbons, and eventually PAHs are formed. Although the details of soot formation are not fully understood, it is generally considered that the first nascent particles (of sizes

CONTACT Sandra Török sandra.torok@forbrf.lth.se; Per-Erik Bengtsson per-erik.bengtsson@forbrf.lth.se Department of Physics, Combustion Physics, Lund University, Box 118, SE-221 00 Lund, Sweden.

Color versions of one or more of the figures in the article can be found online at www.tandfonline.com/uast.

Supplemental data for this article can be accessed on the publisher's website.

1–2 nm) are formed from the stacking of PAHs to three-dimensional structures. These particles grow by surface growth and coagulation, subsequently forming aggregated structures of primary particles (Wang 2011). Over the last decades, a much more detailed understanding of the soot formation processes has been gained from detailed studies in simplified geometries, such as laboratory flames, using combinations of various diagnostic techniques (see, for example, Desgroux et al. 2013). Recently, such studies have focused more intensely on the change of optical properties from the nascent young particles during early soot formation, to the more mature particles later during the soot formation in flames. It has been observed that the soot strongly increases its light absorption during this maturation in flames, which can be related to an increased graphitization of the soot during ageing (Migliorini et al. 2011; Bladh et al. 2011; Cléon et al. 2011; Bejaoui et al. 2015; López-Yglesias et al. 2014; Olofsson et al. 2015; Yon et al. 2011). Another observation from laboratory flame studies is that the wavelength-dependent absorption in the visible (VIS) to near infrared (NIR) spectral regions vary much more strongly for nascent soot than for mature soot, where for mature soot the absorption coefficient K_{abs} approaches the theoretical wavelength dependence and the particles have a close to constant absorption function ($E(m)$) (Simonsson et al. 2015).

The measured absorption coefficient K_{abs} for soot from various experimental works does not always obey a $1/\lambda$-dependence, and more generally the wavelength dependence can be expressed as $K_{abs} \sim 1/\lambda^{AAE}$, where *AAE* is the Absorption Ångström exponent (Schuster et al. 2016; Ångström 1929). By measuring the extinction coefficient, K_{ext}, and using the assumption that we study particles much smaller than the laser wavelength used for the experiments, the scattering contribution will be much smaller than the absorption and hence can be neglected. An alternative approach to express the wavelength dependence of K_{abs} as $K_{abs} \sim 1/\lambda^{AAE}$ is to instead use $K_{abs} \sim E(m,\lambda)/\lambda$, where part of the wavelength-dependent absorption instead is included in the absorption function $E(m,\lambda)$ (López-Yglesias et al. 2014; Migliorini et al. 2011). $E(m,\lambda)$ can be expressed as $E(m,\lambda) = \mathrm{Im}(m^2-1/m^2-2)$, where $m(\lambda)$ is the complex refractive index $m(\lambda) = n - ik$ with n and k as the real and imaginary parts, respectively. The approach of $K_{abs} \sim E(m,\lambda)/\lambda$ is often used in combustion-oriented literature, while the $K_{abs} \sim 1/\lambda^{AAE}$ approach is commonly used for classification of atmospheric aerosols, and the latter approach is also utilized in the present article.

In the recent years, an increased number of investigations have been published dealing with soot produced from soot generators. One soot generator is the so-called miniature combustion aerosol standard (mini-CAST) (Jing 2009), which can generate soot particles with a wide range of physicochemical and optical properties (Schnaiter et al. 2006; Maricq 2014; Moore et al. 2014; Durdina et al. 2016; Kim et al. 2015). Several studies have shown that for many operating conditions, the mini-CAST produces soot that contains large fractions of OC, as determined with thermal-optical analysis. This organic fraction persists to some extent in the soot also after heating (Mamakos et al. 2013; Maricq 2014). Some investigations have focused on optical properties of the mini-CAST soot (Kim et al. 2015; Bescond et al. 2016). In the latter work, a mini-CAST, a PALAS soot generator, and an ethylene flame produced soot with different properties. They observed that the absorption and scattering functions can vary considerably with the soot source, and that the change from an amorphous to a more crystalline structure resulted in increased absorption and scattering capacity (Bescond et al. 2016). In atmospheric sciences, enhanced absorption in the UV/VIS region ($AAE > 1$) is commonly attributed to organic aerosols (coating) only (Saleh et al. 2014; Bond et al. 2013). Flame studies make plausible that enhanced UV/VIS absorption can also (partly) be caused by intrinsic properties of the soot (e.g., the carbon nanostructure) (López-Yglesias et al. 2014; Bescond et al. 2016; Maricq 2014 and references therein). Thus, an aim of this article is to clarify on the nature of BrC emissions, and to what extent the enhanced absorption at short wavelengths (i.e., BrC) evaluated through the *AAE* can be associated with refractory soot components and/or the nonrefractory organic components of the soot.

The focus of this article was to study the optical and physicochemical properties of freshly emitted soot produced at five different operating conditions using a mini-CAST model 5201C. The soot particles generated by the mini-CAST were studied at room temperature and after heat-treatment to 250 and 500°C, in a thermodenuder and tube furnace, respectively. A multiwavelength diode laser *in-situ* extinction setup and an aethalometer were used to study the *AAE*, while a scanning mobility particle sizer (SMPS), thermal-optical carbon analysis, and a soot particle aerosol mass spectrometer (SP-AMS) were used to study the physicochemical properties of the soot. Mini-CAST operating points producing soot with high *AAE* (above 2) were associated with high organic fractions, while operating points producing soot with *AAE* only slightly above 1 had low organic fractions. Heat treatment to 500°C and thereby removal of a large part of the organic aerosol reduced *AAE* to around 2.5, indicating that the refractory particle constituents may give rise to increased

AAE. Finally, we compared the variation of *AAE* for the soot from the mini-CAST operating points with the soot maturation process in premixed laboratory flames.

2. Experimental

2.1. Aerosol generation and processing

An overview of the experimental setup used for our experiments is shown in Figure 1. In order to generate soot particles with various optical and physicochemical properties, a mini-CAST (Jing Ltd, Zollikofen, Switzerland, model 5201C) soot generator (Jing 2009) was used as soot source. The mini-CAST contains a small propane diffusion flame burning with coflow air. The flow of propane and air can be varied ($Q_{air-oxid}$ = 0–2 L min^{-1}, $Q_{propane}$ = 0.02–0.08 L min^{-1}) and consequently the burning characteristics of the flame, such as the flame height. In addition, the flame characteristics were changed by introducing nitrogen (N_2) to be premixed with the propane prior to combustion (Q_{N_2-mix} = 0–0.5 L min^{-1}) causing flame cooling and change of flame height. A second flow of nitrogen quenched the flame at a fixed height above the burner ($Q_{N_2-quench}$ = 7 L min^{-1}), thereby preventing the soot formation process to proceed, and ideally giving soot particles in the exhaust stream representative for the soot at the quenched flame position. During our experiments at room temperature and ambient pressure, we used a selection of the operating points (OP) suggested by the manufacturer (OP1, OP3, OP5, OP6, and OP7), and these are specified in Table 1. The flows presented are the used settings for the internal mass flow controllers of the mini-CAST.

The freshly produced mini-CAST soot was first led through the extinction cell and then diluted prior to the aerosol instruments (SMPS, aethalometer, and SP-AMS). The soot was either studied directly at 25°C (bypass) or initially passing a thermodenuder (TD; Aerodyne Inc. Billerica, MA, USA) at 250°C, or passing the TD at 250°C followed by a ceramic tube furnace (oven) at 500°C (Figure 1). The residence times increased with heat-treatment and are presented in

Table 1. The operating point settings used during the experiments. The fuel (propane) and quench-gas (nitrogen gas) flows were held constant throughout all experiments, while no internal air-dilution was used to minimize the oxygen concentration in the carrier gas and thereby oxidation effects on the soot.

OP	Propane (L min^{-1})	Air-oxid (L min^{-1})	N_2-mix (L min^{-1})	N_2-quench (L min^{-1})	Air-dil (L min^{-1})
1	0.06	1.55	0	7	0
3	0.06	1.52	0.100	7	0
5	0.06	1.47	0.200	7	0
6	0.06	1.42	0.250	7	0
7	0.06	1.36	0.300	7	0

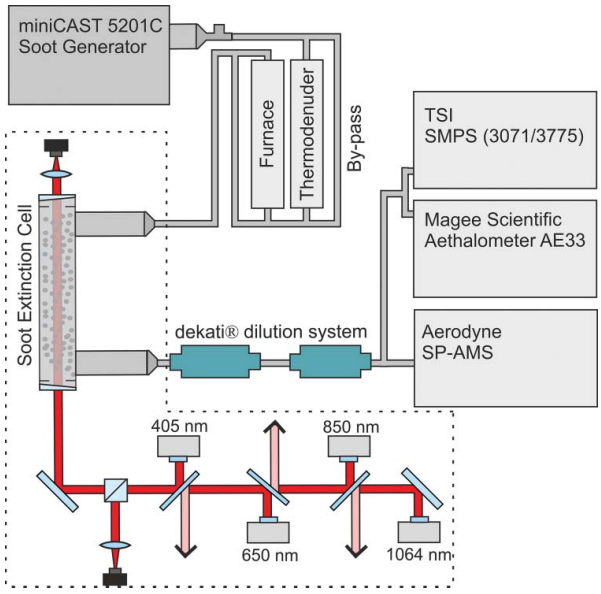

Figure 1. Overview of the experimental setup including the soot preparation system and the measurement devices. The multi-wavelength extinction system and the soot extinction cell is shown in the dashed area.

Table S1 in section S1 in the online supplementary information (SI), and further discussed in connection to Figure 2. After the extinction cell, two ejector diluters (Dekati® diluter) were used in series to dilute the aerosol approximately 1:250 to optimize the conditions for sampling with the aerosol instruments.

2.2. Diagnostic methods

The extinction measurement system was an extended version of a previous system developed for *in-situ* flame measurements (Simonsson et al. 2015), as well as practical combustion and gasification devices (Simonsson et al. 2016). In the present setup a four-wavelength version was used. The extinction setup, presented in the dashed area of Figure 1, shows the four diode lasers (operating at wavelengths 405, 650, 850, and 1,064 nm). The four laser beams were overlapped into one beam and directed through a measurement cell, in which the soot particles suspended in the carrier gas were passing. The four lasers were modulated sequentially at 100 Hz giving a total of 400 laser pulses per second. The laser light was detected using two photodiodes, one placed after the extinction cell to measure the decrease in light intensity, and one acting as a reference detector monitoring the laser intensity prior to the extinction cell to be able to compensate for laser intensity variations. The photodiodes measured at a sampling frequency of 300 kHz. The measurement cell is a 20 cm long, 1″ stainless steel pipe with wedged windows to minimize stray light interferences from window reflections. To ensure minimal soot deposition on

the windows, a small purge flow of nitrogen ($Q_{N_2-purge}$ = 0.1 L min^{-1}) was directed onto the windows. The wavelength dependence of the light extinction is expressed in the form of the *AAE*, which was evaluated by fitting an inverse power law $1/\lambda^{AAE}$ to the extinction data at the four laser wavelengths for each OP case.

In addition to the multiwavelength extinction system, an aethalometer (AE33, Magee Scientific) (Drinovec et al. 2015) was used to measure the light absorption and the *AAE*. The aethalometer operates by depositing soot particles on a filter at two positions at different deposition rates, and measuring the change in attenuation of light at seven wavelengths (370, 470, 520, 590, 660, 880, and 950 nm) through the areas deposited with particles, with time resolution of one second. The compensated aethalometer specific mass absorption cross sections ($MAC_{aethalometer}$) for BC at 880 and 950 nm, 7.77 and 7.19 m^{2}g^{-1}, respectively, were used to obtain the mini-CAST equivalent BC (eBC) concentrations from the aethalometer light absorption data (Drinovec et al. 2015). This method for quantifying the eBC concentrations was validated and showed good agreement with thermal-optical analysis done on the mini-CAST soot samples, as shown in Figure 3a in the results section.

An SP-AMS (Aerodyne Inc. Billerica, MA) (Onasch et al. 2012) was used to probe the chemical composition of the mini-CAST soot. The SP-AMS was switched between standard AMS mode (DeCarlo et al. 2006), i.e., operating in single-vaporizer mode, and SP-AMS mode, i.e., operating in the dual-vaporizer mode. The nonrefractory organic aerosol (including PAHs) was quantified in the standard AMS mode, where particles are vaporized upon impaction on a heated (600°C) tungsten surface. The rBC aerosol was analyzed in the SP-AMS mode (dual vaporizers), where refractory particles are vaporized using an intracavity Nd:YAG laser (at 1,064 nm). In both SP-AMS and AMS mode, vapors are ionized (70 eV electron ionization) and detected in a high-resolution time-of-flight (HR-ToF) mass spectrometer.

Only parent peak PAHs with mass-to-charge ratios (m/z; Th) in the range of m/z 202–300 Th were included in the PAH analysis. The m/z of the included PAHs and the final quantification of particle bound PAH mass is according to a modified version of that described by Herring et al. (2015); Malmborg et al. (2017) and is detailed in section S2 in the SI. Refractory carbon cluster ion fragments originating from the soot core were measured between m/z of 12 and 708 Th (C1−C59). The carbon clusters were divided in three classes: low-carbons (C1–C5), mid-carbons (C6–C29), and fullerene-carbons (C30–C59). Odd-numbered fullerene-carbons contributed with negligible signal to the total fullerene signal.

An SMPS (Electrostatic Classifier model 3071, TSI Inc., and CPC model 3775, TSI Inc.) was used to monitor the size distribution of the studied soot particles. The SMPS was set up with a closed loop sheath flow rate of 3 L min^{-1} and an aerosol flow rate of 0.3 L min^{-1}, giving particle size distributions in the size range of 14 to 697 nm.

Undiluted mini-CAST emissions were collected on quartz filters for thermal-optical (DRI carbon analyzer, model 2001), OC, and elemental carbon (EC) analysis according to the EUSAAR_2 protocol (Cavalli et al. 2010). The EUSAAR_2 protocol was optimized for European regional background sites and divides OC and EC in four subgroups each and a separate group for pyrolytic carbon (PC). OC is evaluated first in an inert He atmosphere and the four subgroups are: OC1 (200°C for 120 s), OC2 (300°C for 150 s), OC3 (450°C for 180 s), OC4 (650°C for 180 s). EC evolves after OC, and is evaluated in He mixed with 2% O_2. The four EC subgroups are: EC1 (500°C for 120 s), EC2 (550°C for 120 s), EC3 (700°C for 70 s), and EC4 (850°C for 80 s). PC, often considered to be a subfraction of OC, corrects the EC measurement for charring effects during the first (OC) analysis. In the final reported EC concentrations, PC was deducted from the measured EC concentrations. TC was calculated as the sum of OC, PC, and EC. Due to failure in the particle sampling on quartz fiber filter of heat-treated (500°C) OP6 soot, carbon fractions at this point were estimated as outlined in section 3 of the SI. An error of 10% (1 std. dev) was estimated for each mass fraction.

3. Results

3.1. Absorption Ångström exponents

In Figure 2a the *AAE* derived from multiwavelength diode laser extinction is shown for OP1, OP3, OP5, OP6, and OP7 for untreated bypass (25°C) soot, thermodenuded soot at 250°C, and furnace-heated soot at 500°C after first being denuded at 250°C. For OP1 and OP3, the *AAE* was evaluated to 1.2, and no significant changes were observed between the results from untreated and the heat-treated soot. The *AAE* increased with OP for cases above OP3, and reached a value $AAE \approx 3.5$ for the untreated soot at OP7. Heating the soot from OP6 and OP7 to 250 and 500°C reduced the *AAE*, in particular for OP7 where *AAE* decreased from 3.5 at 25°C, to 2.8 at 250°C, and finally to 2.5 at 500°C. These *AAE* values are much higher than the values derived for the soot from OP1 and OP3.

The *AAE*s derived from the filter-based aethalometer measurements are shown in Figure 2b. It should be noted that the two different measurement techniques are in very good agreement, which strengthens our results. The good correlation between the data sets is shown in

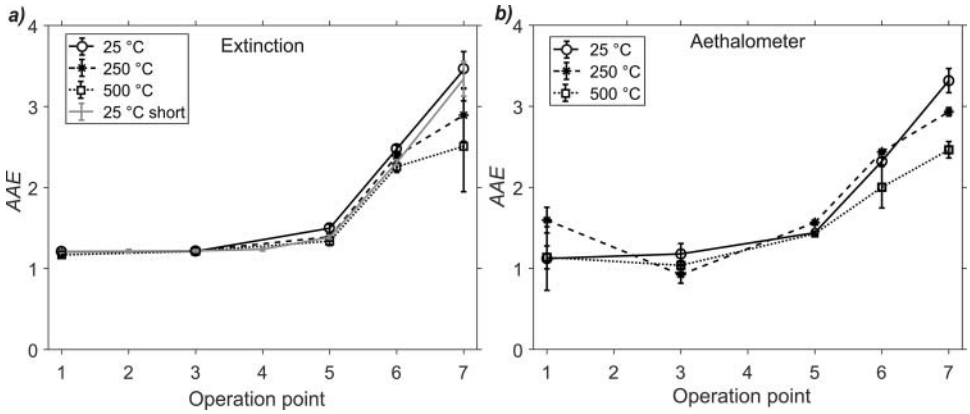

Figure 2. The absorption Ångström exponent (*AAE*) from the mini-CAST operating points with and without heat-treatment from (a) the *in-situ* multiwavelength extinction measurements using four wavelengths and from (b) the aethalometer filter measurements, using seven wavelengths.

section S4 in the SI. However, insufficient correction for the rapid loading of the aethalometer filter for the highly sooting cases (mainly OP1 and OP3) resulted in systematic errors and hence also larger spread in calculated *AAE*s which can be observed in Figure 2b.

Results from a second measurement series at 25°C with a shorter residence time is also shown in Figure 2a. We note that *AAE* for the unheated soot from the short and long residence time remained almost unchanged regardless of residence time and particle sizes for the different OPs (see Section S5 and Figure S3 in the SI for particle size data). Thus, we conclude that the *AAE* only weakly depends on the aggregate size for a given combustion condition in this investigation.

OC, PC, and EC were analyzed by thermal-optical analysis of particles collected on quartz filters. eBC and PAH mass concentrations were derived from the aethalometer (at 880 and 950 nm) and AMS, respectively. The BC fraction measured as eBC to Elemental Carbon ratios (eBC/EC) displayed in Figure 3a show only a weak dependence on OP and are ~1. This result indicates that mass absorption cross sections related to EC (MAC_{EC}) are relatively constant with mini-CAST operating point and heat-treatment. This is consistent with the findings by Durdina et al. (2016) using an array of set-points for two different types of mini-CAST generators. eBC to Total Carbon ratios (eBC/TC) given in Figure 3b were close to 1 at OP1–OP5 but then steeply decreased to around 0.25 at OP7. A similar trend was found when using the mass derived from the SMPS measurements (see Figure S4 in section S6 of the SI). This is consistent with the results derived by Maricq (2014) with similar CAST settings. This also implies that the MAC values related to TC and total particle mass decreases with increasing OP. Taken together, the results shown in Figures 3a and b show that it is very critical which mass fraction is used when calculating BC fractions or MAC values. The EC methods have inherent uncertainties in that the pyrolytic carbon correction depends on the protocol used in the thermal optical analysis.

3.2. Chemical composition of particles

In Figure 3c, the Organic Carbon to Total Carbon ratio (OC/TC) from the thermal optical analysis is given for untreated and heat-treated mini-CAST soot for all OP cases. The OC/TC ratio was low for all OP1–OP5 set points (<0.15) and we observed only minor changes in this ratio when heat-treating the soot. For OP6 and OP7 soot, the OC/TC ratio for the untreated soot was much higher, 0.32 and 0.53, respectively. When heat-treating the soot a decrease in the OC/TC ratio at OP7 was observed. However, OC was still present even at 500°C. This observation of refractory OC is consistent with the previous observations (Makamos et al. 2013; Moore et al. 2014). The OC fractions derived here may be slightly overestimated due to uptake of some gas-phase OC on the quartz fiber filters.

Figure 3d presents the PAH-to-TC ratio (PAH/TC) for untreated and heat-treated mini-CAST soot for all OP cases. The PAH/TC ratio for the soot was <0.015 for OP1, OP3, and OP5. The PAH/TC ratio was higher for untreated OP6 (~0.04) and OP7 (~0.06) soot. Heat-treating to 250 and 500°C removed two-thirds of the PAHs at OP6. At OP7, heat-treating to 250°C removed approximately 50% of the PAHs, while at 500°C close to 90% of the PAHs were evaporated.

For the soot with high *AAE*, organic aerosol mass (OA including PAHs) sampled with the AMS were collectively significantly lower than derived OC masses (both with respect to OC and ∑OC+PC) (see Figure S5 in Section S7 of the SI). The reason for this

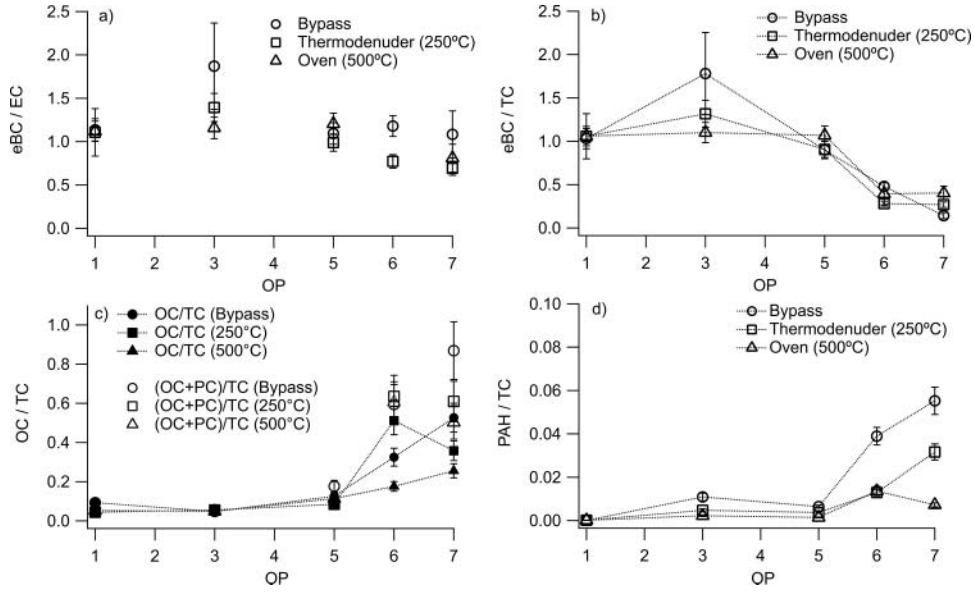

Figure 3. (a) eBC-to-EC ratios showing values close to 1 for all operating points (OP) and temperatures. (b) eBC-to-TC ratios decreasing with OP. (c) OC-to-TC and OC+PC-to-TC ratios increasing with OP and decreasing after heat-treating. (d) PAH-to-TC ratios. The error bars show ±1 STD.

disagreement is not clear; it is partly caused by gas phase adsorption to the quartz fiber filters used for OC/EC. AMS-derived OA masses were on the same order and in fairly good agreement with the thermal-optically derived OC1 and OC2 masses. Failure to detect part of the material classified as OC3–4 and PC with AMS flash vaporization (600°C Tungsten surface in vacuum) may indicate that OC3–4 and PC from mini-CAST soot cannot be easily separated from EC. It could potentially also be explained by particle bounce off the AMS-vaporizer, which can lead to underestimations in the AMS mass quantification (Matthew et al. 2008). We hypothesize that the components classified as OC and PC that cannot be detected with the AMS may comprise the highly amorphous nanostructures associated with immature soot, and are therefore partly incorporated into the soot carbon-matrix.

Except for PAHs, which can have significant absorption at shorter UV–VIS wavelengths, the nonrefractory mass spectra from AMS were dominated by aliphatic fragments that are commonly associated with diesel vehicle emissions and low absorptivity (Zhang et al. 2005). Additional "brown" absorption was, therefore, likely confined to the OC3–4, PC, and EC that did not evaporate after heat-treating the soot to 500°C.

3.3. Comparison of mass spectra from refractory soot properties (SP-AMS)

Refractory mass spectra originating from the soot were obtained with dual vaporizers in the SP-AMS mode. The refractory mass spectra of carbon clusters (rC_x^+) were dominated by low-carbons (C_1^+–C_5^+) for OP1 and OP3. For OP5, OP6, and OP7, the signal from larger carbon clusters, 12 Th-spaced mid-carbons (C_6^+–C_{29}^+) and 24 Th-spaced fullerene-carbons (C_{30}^+–C_{58}^+) increased dramatically. Figure 4 shows the refractory carbon cluster

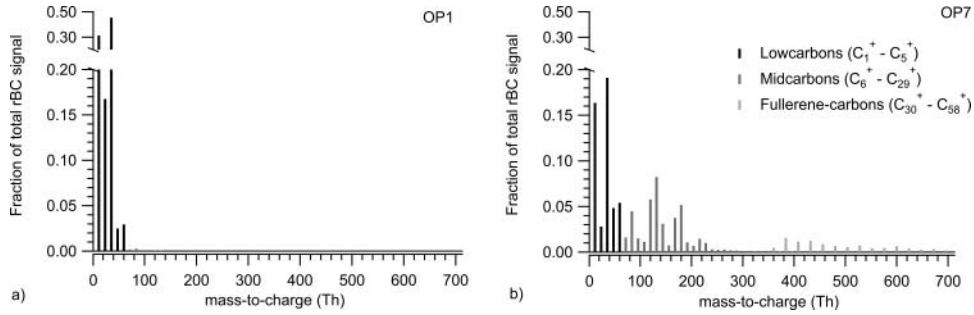

Figure 4. rBC carbon ion cluster distribution in laser vaporizer SP-AMS mass spectra of: (a) OP1 soot and (b) OP7 soot.

distribution of OP1 and OP7 (at 25°C). Mid- and fullerene-carbons had marginal contributions to the total rBC signal for OP1 soot, while at OP7 they contributed with more than 50% of the total carbon signal. The carbon cluster distributions have previously been hypothesized to be related to the maturity or carbon nanostructure of the soot (Malmborg et al. 2017; Maricq 2014; Onasch et al. 2015). Low carbons commonly dominate mature (graphitized) soot (e.g., diesel exhaust soot) (Onasch et al. 2015), while larger carbon clusters have been observed in premixed flames, fullerene-soot (Onasch et al. 2015), and early in the diesel engine combustion cycle (i.e., immature diesel soot) (Malmborg et al. 2017). Variations in the refractory carbon cluster distribution, and the occurrence of 24 Th-spaced carbon cations at fullerene-sized clusters, have previously been reported for mini-CAST soot (Maricq 2014).

Heat-treating the soot up to 500°C to remove the volatile particle fraction had only marginal influence on the SP-AMS refractory mass spectra for all OP cases. This indicates that the refractory part of the soot was not altered significantly by the heat-treatment, i.e., the large differences in mass spectra for OP1 and OP7 shown in Figure 4 remained after heat treatment. Hence, observed changes in *AAE* with heat-treatment can be assigned primarily to the volatile OA evaporation.

3.4. Relating enhanced absorption at shorter wavelengths to particle composition

The BC fractions (and thereby MAC values) decreased strongly with OP with respect to the total particle mass. So the simplest model looking only at average particle composition and optical properties shows that *AAE* increases and MAC_{TC}(950 nm) decreases with increasing OP, both before and after heat treatment. After heating soot from OP6 and OP7, the *AAE* decreased significantly but remained at values much higher than 1.0. Simultaneously with the decrease in *AAE*, PAHs were almost completely evaporated from the soot at the highest temperature. However, the thermal-optical analysis revealed that large fractions quantified as organic and pyrolytic carbon could not be removed when heat-treating the soot to 500°C. In this section, we investigate whether or not these components can explain the additional absorption at shorter wavelengths for the OP soot with high *AAE*. The estimations made are based on the measured absorption at 950 and 520 nm, OC, PC, and EC masses, and finally the assumption that *AAE* for EC (AAE_{EC}) may deviate from 1.

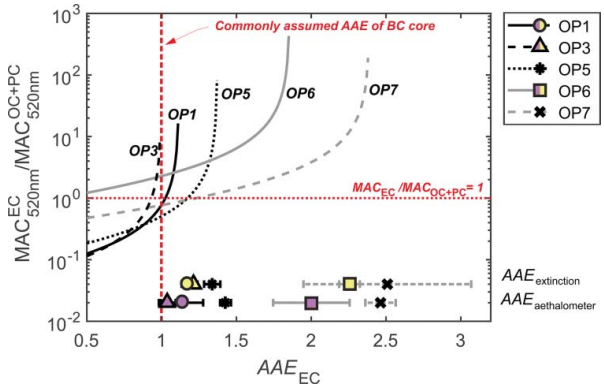

Figure 5. The ratio between MAC(520 nm) for EC and ∑OC+PC as a function of the AAE for the EC is shown. As EC commonly is assumed to have AAE ~ 1, this value is marked as a dashed vertical line. Also the lower limit for a realistic MAC ratio between EC and ∑OC+PC is marked with the horizontal dashed line. In the bottom part of the figure, the measured AAE from both extinction and aethalometer measurements are presented for comparison.

The simulations are displayed in Figure 5. The figure was derived from Equation (1) using the experimental wavelength-dependent absorption coefficient for the entire soot particles, $K^{TOT}_{abs}(\lambda)$, the mass concentrations for EC (m_{EC}), and ∑OC+PC (m_{OC+PC}) for all OP cases after heat-treatment to 500°C, and the assumption that absorption from OC+PC is negligible at the highest aethalometer wavelength (950 nm). Hence, the experimental wavelength-dependent absorption coefficient for the EC, $K^{EC}_{abs}(950\ nm) = K^{TOT}_{abs}(950\ nm)$. The latter assumption is based on the good agreement between eBC and EC shown in Figure 3a. This allows K_{abs} for EC and ∑OC+PC to be calculated separately. From Equation (1), the MAC ratio between EC and ∑OC+PC fractions as a function of AAE_{EC} is obtained for a specific wavelength (λ).

$$\frac{MAC^{EC}_{\lambda}}{MAC^{OC+PC}_{\lambda}} = \frac{K^{EC}_{abs}(AAE_{EC},\ \lambda)\ /\ m_{EC}}{\left(K^{TOT}_{abs}(\lambda) - K^{EC}_{abs}(AAE_{EC},\ \lambda)\right)\ /\ m_{OC+PC}} \quad [1]$$

According to e.g., Bond et al. (2013), MAC_{BC} should be at least 7.5 times MAC_{OA} at 550 nm. However, we chose to evaluate MAC at 520 nm as it is one of the aethalometer wavelengths and of atmospheric relevance. We propose that MAC_{EC} to MAC_{OC+PC} ratios lower than 1 are nonrealistic. This sets a lower limit to AAE_{EC} (dashed lower line in Figure 5).

The results of the simulation show that MAC_{EC} to MAC_{OC+PC} ratios are above 1 for all OPs when $AAE_{EC} > 1.3$. With the current method, it is not possible to determine the value of AAE_{EC}. It is, therefore,

still possible that AAE_{EC} is closer to the *AAE* of the aerosol (~2 for OP6 and ~2.5 for OP7). If AAE_{EC} were indeed closer to 1, a significant part of the absorption at short wavelengths would be assigned to the OC and PC fractions which could not be removed by heat-treating to 500°C. The difficulty to evaporate these species and the difficulty to detect them with the AMS (operated at 600°C vaporization) shows that the soot with high *AAE* may not be described by a traditional refractory, strongly absorbing soot-core and nonrefractory, weakly absorbing soot-coating model. Efficiently absorbing OC and PC may instead be intrinsically mixed with EC and represent amorphous soot carbon-nanostructures found in high-resolution transmission electron microscopy (HR-TEM) analyses, and be related to the presence of large carbon clusters in the SP-AMS analysis.

3.5. Optical properties of mini-CAST soot in relation to in-situ *flame soot*

High *AAE*s (>1.5) were in previous chapters associated with high organic and pyrolytic carbon fractions of the mini-CAST soot. These organics were not removed by heating the aerosol to 500°C in a ceramic tube furnace (and thermodenuder). These results make a comparison to the change of optical properties during the soot formation process in a flame interesting. In a previous study, soot was studied through extinction measurements at 12 wavelengths as a function of height above burner (HAB) in premixed ethylene/air flames (Simonsson et al. 2015). In these flames, the soot nucleation starts at around 4 mm HAB, and then the soot particles grow by surface growth and coagulation when transported upwards in the flame. Evaluations of *AAE* at different wavelengths are shown in Figure 6. It can be observed that the evaluated *AAE* changes from high values (3 to 4) at low HAB and decreases towards higher flame positions (final *AAE* in the range 1.3–1.4). The hollow circles represent evaluations based on 12 wavelengths in the range from 405–1,064 nm. In the present work on mini-CAST soot, only four wavelengths were used in our experimental setup. These four wavelengths were used in a reevaluation of the data, presented in Figure 6, marked as crosses. The four-wavelength evaluation gives results in good agreement with the 12-wavelength evaluation, especially at the higher flame heights. A third evaluation is also presented (as dots) in Figure 6, in which only the wavelengths in the range 685–1,064 nm were used. For this evaluation, *AAE* approaches a value of 1 at higher flame heights which is the theoretical value for absorption from small particles using the Rayleigh criterion and a wavelength-independent $E(m)$. The similarities between the optical properties of mini-CAST soot and in-flame soot at various HAB indicate that the variations in mini-CAST soot properties can be closely related to different levels of soot maturity, and physicochemical properties found in emissions with elevated *AAE* of other combustion sources.

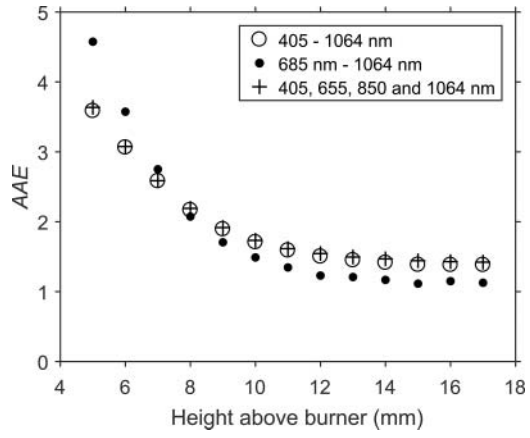

Figure 6. AAE for soot in an $\Phi = 2.3$ premixed McKenna flame as function of height above burner (5–17 mm). The hollow circles show the AAE evaluated using the extinction at 12 wavelengths between 405 and 1,064 nm, the black dots using the wavelengths above 685 nm and the crosses using the same wavelengths used as in our mini-CAST experiments.

4. Conclusions

The main conclusions from this study on optical and physicochemical properties of mini-CAST soot are the following:

- Good agreement was found in measured *AAE* between *in-situ* multiwavelength extinction and filter-based aethalometer data for all types of mini-CAST soot with and without heat treatment.
- The soot types from the various OP cases showed increasing *AAE* with increasing OC+PC fraction. For soot with an *AAE* close to 1 (~1.2), heating had negligible impact on the measured *AAE* and the already low OC fraction. For soot with a high *AAE* (~3.5), heating resulted in a decreasing OC fraction and decreasing *AAE*. However, even with heating to 500°C the *AAE* remained high (up to 2.5) and evidence of persistent OC and PC was found.
- Estimations of the absorption (at 520 nm) from the different soot constituents indicated that high *AAE*s were at least partly caused by the persistent OC and PC constituents.
- The differences in refractory soot mass spectra from SP-AMS data indicate that the refractory soot

bonding structure is different for soot with high and low OC+PC fractions.

- Comparison of the measured *AAE* of the studied soot with soot during formation in 1D premixed flames (Simonsson et al. 2015) suggests that the soot with a large OC+PC fraction (high OP cases) is of less mature character than soot with small OC+PC fraction (low OP cases), as also discussed by Maricq (2014).

From the results of this study, we hypothesized that the selected mini-CAST soot types span from small particles of immature character, to larger soot particles of mature character. Smaller, immature particles had high *AAE*s and OC and PC fractions that remained high even after heating the soot to 500°C. Larger, mature soot particles had *AAE*s close to 1, low OC fraction, and no PC. The observations support that the high *AAE*s associated with certain mini-CAST operating points were not only caused by semivolatile organics (e.g., PAHs), but resulted from absorption by the OC and PC components persistent after heating to 500°C and/or enhanced absorption by the EC at shorter wavelengths. In combination with the latter findings, the wide distribution of refractory carbon clusters found in SP-AMS mass spectra of these particles can suggest that OC, PC, and EC fractions for the immature particles are not well described by a soot core and coating model.

Funding

The work received financial support from the Swedish Research Council Formas [2013–453] and the Swedish Research Council VR [2013–5021].

References

Ångström, A. (1929). On the Atmospheric Transmission of Sun Radiation and on Dust in the Air. *Geografiska Annaler*, 11:156–166.

Bejaoui, S., Batut, S., Therssen, E., Lamoureux, N., Desgroux, P., and Liu, F. (2015). Measurements and Modeling of Laser-Induced Incandescence of Soot at Different Heights in a Flat Premixed Flame. *Appl. Phys. B.*, 118:449–469. doi:10.1007/s00340-015-6014-3.

Bescond, A., Yon, J., Ouf, F.-X., Rozé, C., Coppalle, A., Parent, P., Ferry, D., and Laffon, C. (2016). Soot Optical Properties Determined by Analyzing Extinction Spectra in the Visible Near-UV: Toward an Optical Speciation According to Constituents and Structure. *J. Aerosol Sci.*, 101:118–132. doi:10.1016/j.jaerosci.2016.08.001.

Bladh, H., Johnsson, J., Olofsson, N.-E., Bohlin, A., and Bengtsson, P.-E. (2011). Optical Soot Characterization Using Two-Color Laser-Induced Incandescence (2C-LII) in the Soot Growth Region of a Premixed Flat Flame. *Proc. Combust. Inst.*, 33:641–648. doi:10.1016/j.proci.2010.06.166.

Bockhorn, H. (2013). *Soot Formation in Combustion: Mechanisms and Models*. Vol. 59. Springer Science & Business Media, Berlin and Heidelberg, Germany.

Bond, T. C. and Bergstrom, R. W. (2006). Light Absorption by Carbonaceous Particles: An Investigative Review. *Aerosol Sci. Technol.*, 40:27–67. doi:10.1080/02786820500421521.

Bond, T. C., Doherty, S. J., Fahey, D. W., Forster, P. M., Berntsen, T., DeAngelo, B. J., Flanner, M. G., Ghan, S., Kärcher, B., Koch, D., Kinne, S., Kondo, Y., Quinn, P. K., Sarofim, M. C., Schultz, M. G., Schulz, M., Venkataraman, C., Zhang, H., Zhang, S., Bellouin, N., Guttikunda, S. K., Hopke, P. K., Jacobson, M. Z., Kaiser, J. W., Klimont, Z., Lohmann, U., Schwarz, J. P., Shindell, D., Storelvmo, T., Warren, S. G., and Zender, C. S. (2013). Bounding the Role of Black Carbon in the Climate System: A Scientific Assessment. *J. Geophys. Res.: Atmos.*, 118:5380–5552.

Boström, C.-E., Gerde, P., Hanberg, A., Jernström, B., Johansson, C., Kyrklund, T., Rannug, A., Törnqvist, M., Victorin, K., and Westerholm, R. (2002). Cancer Risk Assessment, Indicators, and Guidelines for Polycyclic Aromatic Hydrocarbons in the Ambient Air. *Environ. Health Perspect.*, 110:451–488. doi:10.1289/ehp.02110s3451.

Canagaratna, M. R., Massoli, P., Browne, E. C., Franklin, J. P., Wilson, K. R., Onasch, T. B., Kirchstetter, T. W., Fortner, E. C., Kolb, C. E., Jayne, J. T., Kroll, J. H., and Worsnop, D. R. (2015). Chemical Compositions of Black Carbon Particle Cores and Coatings via Soot Particle Aerosol Mass Spectrometry with Photoionization and Electron Ionization. *J. Phys. Chem. A.*, 119:4589–4599. doi:10.1021/jp510711u.

Cappa, C. D., Onasch, T. B., Massoli, P., Worsnop, D. R., Bates, T. S., Cross, E. S., Davidovits, P., Hakala, J., Hayden, K. L., Jobson, B. T., Kolesar, K. R., Lack, D. A., Lerner, B. M., Li, S.-M., Mellon, D., Nuaaman, I., Olfert, J. S., Petäjä, T., Quinn, P. K., Song, C., Subramanian, R., Williams, E. J., and Zaveri, R. A. (2012). Radiative Absorption Enhancements Due to the Mixing State of Atmospheric Black Carbon. *Science*, 337:1078–1081. doi:10.1126/science.1223447.

Cavalli, F., Viana, M., Yttri, K. E., Genberg, J., and Putaud, J.-P. (2010). Toward a Standardised Thermal-Optical Protocol for Measuring Atmospheric Organic and Elemental Carbon: The EUSAAR Protocol. *Atmos. Meas. Tech.*, 3:79–89. doi:10.5194/amt-3-79-2010.

Cléon, G., Amodeo, T., Faccinetto, A., and Desgroux, P. (2011). Laser Induced Incandescence Determination of the Ratio of the Soot Absorption Functions at 532 nm and 1064 nm in the Nucleation Zone of a Low Pressure Premixed Sooting Flame. *Appl. Phys. B: Lasers Optics*, 104:297–305. doi:10.1007/s00340-011-4372-z.

DeCarlo, P. F., Kimmel, J. R., Trimborn, A., Northway, M. J., Jayne, J. T., Aiken, A. C., Gonin, M., Fuhrer, K., Horvath, T., and Docherty, K. S. (2006). Field-Deployable, High-Resolution, Time-of-Flight Aerosol Mass Spectrometer. *Anal. Chem.*, 78:8281–8289. doi:10.1021/ac061249n.

Desgroux, P., Mercier, X., and Thomson, K. A. (2013). Study of the Formation of Soot and Its Precursors in Flames Using Optical Diagnostics. *Proc. Combust. Inst.*, 34:1713–1738. doi:10.1016/j.proci.2012.09.004.

Drinovec, L., Močnik, G., Zotter, P., Prévôt, A. S. H., Ruckstuhl, C., Coz, E., Rupakheti, M., Sciare, J., Müller, T., Wiedensohler, A., and Hansen, A. D. A. (2015). The "Dual-Spot"

Aethalometer: An Improved Measurement of Aerosol Black Carbon with Real-Time Loading Compensation. *Atmos. Meas. Tech.*, 8:1965–1979. doi:10.5194/amt-8-1965-2015.

Durdina, L., Lobo, P., Trueblood, M. B., Black, E. A., Achterberg, S., Hagen, D. E., Brem, B. T., and Wang, J. (2016). Response of Real-Time Black Carbon Mass Instruments to Mini-CAST Soot. *Aerosol Sci. Technol.*, 50:906–918. doi:10.1080/02786826.2016.1204423.

Herring, C. L., Faiola, C. L., Massoli, P., Sueper, D., Erickson, M. H., McDonald, J. D., Simpson, C. D., Yost, M. G., Jobson, B. T., and VanReken, T. M. (2015). New Methodology for Quantifying Polycyclic Aromatic Hydrocarbons (PAHs) Using High-Resolution Aerosol Mass Spectrometry. *Aerosol Sci. Technol.*, 49:1131–1148. doi:10.1080/02786826.2015.1101050.

IPCC. (2013). *Climate Change 2013: The Physical Science Basis. Contribution of Working Group I to the Fifth Assessment Report of the Intergovernmental Panel on Climate Change*. Cambridge University Press, Cambridge, United Kingdom and New York, NY, USA.

Janssen, N. A. H., Gerlofs-Nijland, M. E., Lanki, T., Salonen, R. O., Cassee, F., Hoek, G., Fischer, P., Brunekreef, B., and Krzyzanowski, M. (2012). *Health Effects of Black Carbon*. WHO, Copenhagen, Denmark.

Jing. (2009). Mini-CAST Soot Generator. Accessed February 14. http://www.sootgenerator.com/.

Kennedy, I. M. (2007). The Health Effects of Combustion-Generated Aerosols. *Proc. Combust. Inst.*, 31:2757–2770. doi:10.1016/j.proci.2006.08.116.

Kim, J., Bauer, H., Dobovičnik, T., Hitzenberger, R., Lottin, D., Ferry, D., and Petzold, A. (2015). Assessing Optical Properties and Refractive Index of Combustion Aerosol Particles Through Combined Experimental and Modeling Studies. *Aerosol Sci. Technol.*, 49:340–350. doi:10.1080/02786826.2015.1020996.

Liu, D., Whitehead, J., Alfarra, M. R., Reyes-Villegas, E., Spracklen, D. V., Reddington, C. L., Kong, S., Williams, P. I., Ting, Y.-C., Haslett, S., Taylor, J. W., Flynn, M. J., Morgan, W. T., McFiggans, G., Coe, H., and Allan, J. D. (2017). Black-Carbon Absorption Enhancement in the Atmosphere Determined by Particle Mixing State. *Nat. Geosci.*, 10:184–188. doi:10.1038/ngeo2901.

Liu, S., Aiken, A. C., Gorkowski, K., Dubey, M. K., Cappa, C. D., Williams, L. R., Herndon, S. C., Massoli, P., Fortner, E. C., and Chhabra, P. S. (2015). Enhanced Light Absorption by Mixed Source Black and Brown Carbon Particles in UK Winter. *Nat. Commun.*, 6:1–10. Article No. 8435. doi:10.1038/ncomms9435.

López-Yglesias, X., Schrader, P. E., and Michelsen, H. A. (2014). Soot Maturity and Absorption Cross Sections. *J. Aerosol Sci.*, 75:43–64. doi:10.1016/j.jaerosci.2014.04.011.

Malmborg, V. B., Eriksson, A. C., Shen, M., Nilsson, P., Gallo, Y., Waldheim, B., Martinsson, J., Andersson, O., and Pagels, J. (2017). Evolution of In-Cylinder Diesel Engine Soot and Emission Characteristics Investigated with On-Line Aerosol Mass Spectrometry. *Environ. Sci. Technol.*, 51:1876–1885. doi:10.1021/acs.est.6b03391.

Mamakos, A., Khalek, I., Giannelli, R., and Spears, M. (2013). Characterization of Combustion Aerosol Produced by a Mini-CAST and Treated in a Catalytic Stripper. *Aerosol Sci. Technol.*, 47:927–936. doi:10.1080/02786826.2013.802762.

Maricq, M. M. (2014). Examining the Relationship Between Black Carbon and Soot in Flames and Engine Exhaust. *Aerosol Sci. Technol.*, 48:620–629. doi:10.1080/02786826.2014.904961.

Matthew, B. M., Middlebrook, A. M., and Onasch, T. B. (2008). Collection Efficiencies in an Aerodyne Aerosol Mass Spectrometer as a Function of Particle Phase for Laboratory Generated Aerosols. *Aerosol Sci. Technol.*, 42:884–898. doi:10.1080/02786820802356797.

Migliorini, F., Thomson, K. A., and Smallwood, G. J. (2011). Investigation of Optical Properties of Aging Soot. *Appl. Phys. B: Lasers Optics*, 104:273–283. doi:10.1007/s00340-011-4396-4.

Moore, R. H., Ziemba, L. D., Dutcher, D., Beyersdorf, A. J., Chan, K., Crumeyrolle, S., Raymond, T. M., Thornhill, K. L., Winstead, E. L., and Anderson, B. E. (2014). Mapping the Operation of the Miniature Combustion Aerosol Standard (Mini-CAST) Soot Generator. *Aerosol Sci. Technol.*, 48:467–479. doi:10.1080/02786826.2014.890694.

Olofsson, N.-E., Simonsson, J., Török, S., Bladh, H., and Bengtsson, P.-E. (2015). Evolution of Properties for Aging Soot in Premixed Flat Flames Studied by Laser-Induced Incandescence and Elastic Light Scattering. *Appl. Phys. B*, 119:669–683. doi:10.1007/s00340-015-6067-3.

Onasch, T. B., Fortner, E. C., Trimborn, A. M., Lambe, A. T., Tiwari, A. J., Marr, L. C., Corbin, J. C., Mensah, A. A., Williams, L. R., and Davidovits, P. (2015). Investigations of SP-AMS Carbon Ion Distributions as a Function of Refractory Black Carbon Particle Type. *Aerosol Sci. Technol.*, 49:409–422. doi:10.1080/02786826.2015.1039959.

Onasch, T. B., Trimborn, A., Fortner, E. C., Jayne, J. T., Kok, G. L., Williams, L. R., Davidovits, P., and Worsnop, D. R. (2012). Soot Particle Aerosol Mass Spectrometer: Development, Validation, and Initial Application. *Aerosol Sci. Technol.*, 46:804–817. doi:10.1080/02786826.2012.663948.

Saleh, R., Robinson, E. S., Tkacik, D. S., Ahern, A. T., Liu, S., Aiken, A. C., Sullivan, R. C., Presto, A. A., Dubey, M. K., and Yokelson, R. J. (2014). Brownness of Organics in Aerosols from Biomass Burning Linked to Their Black Carbon Content. *Nat. Geosci.*, 7:647–650. doi:10.1038/ngeo2220.

Schnaiter, M., Gimmler, M., Llamas, I., Linke, C., Jäger, C., and Mutschke, H. (2006). Strong Spectral Dependence of Light Absorption by Organic Carbon Particles Formed by Propane Combustion. *Atmos. Chem. Phys.*, 6:2981–2990. doi:10.5194/acp-6-2981-2006.

Schuster, G. L., Dubovik, O., Arola, A., Eck, T. F., and Holben, B. N. (2016). Remote Sensing of Soot Carbon— Part 2: Understanding the Absorption Ångström Exponent. *Atmos. Chem. Phys.*, 16:1587–1602. doi:10.5194/acp-16-1587-2016.

Simonsson, J., Bladh, H., Gullberg, M., Pettersson, E., Sepman, A., Ögren, Y., Wiinikka, H., and Bengtsson, P.-E. (2016). Soot Concentrations in an Atmospheric Entrained Flow Gasifier with Variations in Fuel and Burner Configuration Studied Using Diode-Laser Extinction Measurements. *Energy Fuels*, 30:2174–2186. doi:10.1021/acs.energyfuels.5b02561.

Simonsson, J., Olofsson, N.-E., Török, S., Bengtsson, P.-E., and Bladh, H. (2015). Wavelength Dependence of Extinction in Sooting Flat Premixed Flames in the Visible and Near-Infrared Regimes. *Appl. Phys. B*, 119:657–667. doi:10.1007/s00340-015-6079-z.

Wang, H. (2011). Formation of Nascent Soot and Other Condensed-Phase Materials in Flames. *Proc. Combust. Inst.*, 33:41–67. doi:10.1016/j.proci.2010.09.009.

Yon, J., Lemaire, R., Therssen, E., Desgroux, P., Coppalle, A., and Ren, K. F. (2011). Examination of Wavelength Dependent Soot Optical Properties of Diesel and Diesel/Rapeseed Methyl Ester Mixture by Extinction Spectra Analysis and LII Measurements. *Appl. Phys. B*, 104:253–271. doi:10.1007/s00340-011-4416-4.

Zhang, Q., Worsnop, D. R., Canagaratna, M. R., and Jimenez, J. L. (2005). Hydrocarbon-Like and Oxygenated Organic Aerosols in Pittsburgh: Insights into Sources and Processes of Organic Aerosols. *Atmos. Chem. Phys.*, 5:3289–3311. doi:10.5194/acp-5-3289-2005.